Kinetic Study of Higher Alcohol Synthesis Directly from Syngas over $CoCu/SiO_2$ Catalysts

Junjie Su, Wei Mao, Xin-Chao Xu, Zhen Yang, Honglin Li, Jing Xu, and Yi-Fan Han
State Key Laboratory of Chemical Engineering, East China University of Science and Technology, Shanghai 200237, China

DOI 10.1002/aic.14354
Published online January 23, 2014 in Wiley Online Library (wileyonlinelibrary.com)

Higher alcohol synthesis (HAS) directly from syngas is one of the most promising approaches for utilizing nonoil resources cleanly and efficiently. A series of bimetallic CoCu catalysts with different Co/Cu ratios were prepared using a SiO_2 support. The structure of Cu modified Co catalysts was characterized using HRTEM, in/ex situ X-ray diffraction, and temperature-programmed reduction. It was evidenced that nanoscale metal particles were formed and the reduction of Co oxide at above 673 K. Meanwhile, the interaction between Co and Cu on the surface was assumed to be responsible for the enhanced selectivity to HAS. The intrinsic kinetics for this reaction was performed over a $CoCu/SiO_2$ catalyst under realistic conditions. The kinetic parameters, including apparent activation energies and reaction orders, were calculated through power-law models. With the combination of chain growth probability and kinetics, the effect of temperatures on the reaction mechanism and the Cu promotional effects on Co catalysts were elaborated. © 2014 American Institute of Chemical Engineers *AIChE J*, 60: 1797–1809, 2014
Keywords: higher alcohol synthesis, intrinsic kinetics, syngas, bimetallic CoCu catalysts, surface alloy

Introduction

With the dwindling of crude oil resources, the production of fuels and chemicals via alternative energy sources is becoming an important issue for the sustainable world economics.[1,2] It has been reported that for the total fossil fuel reserves, the crude oil only takes up about 6.6% while the rest is coal, sand oil, and natural (shale) gas.[3] The production of synthetic fuels based on those nonoil raw materials has been attracting to industry for almost 90 years since the well-known Fischer–Tropsch (F–T) process was developed in Germany in the early part of the last century as a way to produce liquid fuels, such as diesel, from coal.[4] It is now possible to use feedstocks such as natural gas and biogas for the production of synthetic fuels. The range of products is broad and includes diesel, jet fuel, naphtha, and bases for synthetic lubricants, varied with the property of catalysts and the reaction conditions.[5–7] Generally, these are of higher quality with less sulfur or aromatics than those derived from conventional means.

In the F–T process, fossil fuels are first converted to synthesis gas (syngas) consisting of carbon monoxide (CO) and hydrogen (H_2) through a gasification process; hydrocarbons can then be produced via catalytic reactions. In particular, high value-added chemicals such as alcohols and olefins, or to say "light weight hydrocarbons," can be produced as well; those chemicals can be a primary products over particular catalysts under well-controlled conditions.[8] The higher alcohols (other than methanol) from syngas chemistry own several advantages, such as high octane number as gasoline blends or motor fuels, containing no sulfur and aromatic hydrocarbons, thus making them both environmentally and economically valuable.[9–11]

Different types of catalysts have been developed for this process, including rhodium-based noble metal catalysts,[12] molybdenum sulfide-based catalysts,[13] modified F–T catalysts,[14] and modified methanol synthesis catalysts.[15] Rhodium-based catalysts exhibited higher selectivity and activity to oxygenates, especially C_2 oxygenates (ethanol, acetaldehyde, and acetic acid),[1] but it is still unfeasible for practical applications because of its high cost and low efficiency. In comparison, molybdenum-based catalysts proved to have excellent sulfur resistance[16]; however, the low activity and harsh reaction conditions (ca. 10.0 MPa) limited its industrial application.[11,17] Methanol synthesis catalysts include Zn—Cr and Cu—Zn—Al based catalysts, on which the selectivity to higher alcohols mainly composed of branched alcohols was rather low.[18,19] On the contrary, C_1—C_5 linear alcohols found to be the main products over modified F–T catalysts such as cobalt-based catalysts.[17,20,21] This is the most promising process for industrialization in virtue of mild reaction conditions; in particular, among all modified Co catalysts, bimetallic Cu—Co catalysts have received the most attentions because of their better durability for this process, originally developed by the French Petroleum Institute.[22,23]

Earlier works of CO hydrogenation over Co-based catalysts have already been reviewed.[24,25] Co catalysts modified

Additional Supporting Information may be found in the online version of this article.

Correspondence concerning this article should be addressed to Y.-F. Han at yifanhan@ecust.edu.cn.

© 2014 American Institute of Chemical Engineers

by Cu showed higher selectivity toward alcohols, meanwhile bimetallic phase generated via the reduction of $CuCo_2O_4$ with spinel structure was assumed to be the active site for higher alcohol synthesis (HAS).[20,21,26–28] As the bulk CoCu alloy is unlikely formed due to the low solubility of both metals,[29] it is still unclear the interaction between Co and Cu in bimetallic Co—Cu catalysts and the way Cu atoms take effects on HAS. A more recent study by Smith et al.[30] revealed that the dispersion of Co and Cu could be improved simultaneously while the reduction of $CuO \rightarrow Cu^0$ and $Co_3O_4 \rightarrow CoO$ was greatly enhanced. Carenco et al.[31] suggested that Co and Cu could each individually contribute to syngas conversion using bimetallic CoCu catalysts. Unfortunately, to the best of our knowledge, up to now the detailed kinetic study of this reaction system under the real reaction conditions, which is the only way to reflect the catalytic behavior and rationalize the plausible mechanism, is still very rare, except for a few early works for F–T process over unmodified Co catalysts[32] and a recent steady-state isotopic transient kinetic analysis over a Co/Cu/ZnO catalyst under methanation conditions in a high ratio of $H_2/CO = 30$.[33]

In the present study, as a part of our efforts to the mechanistic study of the aiming reaction system, the intrinsic kinetics for HAS directly from syngas was studied using a series of Co—Cu/SiO_2 catalysts prepared by an impregnation method in a microfixed-bed reactor. The texture property of supported bimetallic CoCu nanoparticles was characterized using transmission electron microscopy (TEM), *ex situ* and *in situ* X-ray diffraction (XRD), and N_2 adsorption. The temperature-programmed reduction (TPR) was also performed for the determination of the interaction between Cu and Co. Later, the kinetic measurements of CO hydrogenation in the temperature range 513–553 K were carried out over the catalyst with an optimum composition; meanwhile, the analytic method for determining the products was established.

The present study will shed deep insight into the creation of active sites on Cu modified Co F–T synthesis catalysts, especially, for HAS. We believe the kinetic parameters measured under real operating conditions are valuable for both industry by design of reactor and academia by exploration of reaction mechanism.

Experimental

Catalyst preparation

All catalysts were prepared by an incipient wetness method using a silica gel as the support (Brunauer-Emmett-Teller (BET) surface area of 304 m^2/g, Qingdao Makall Group, China), which proved to be inert to syngas conversion. In this process, silica gel was first washed with nitric acid to remove metal impurities, and then washed with deionized water until the solution became neutral. Then, silica gel was dried at 383 K for 10 h and calcined in air at 623 K for 3 h. Finally, the support was ground and sieved to specific size needed for use. The aqueous solution with $Cu(NO_3)_2{\cdot}3H_2O$ and $Co(NO_3)_2{\cdot}6H_2O$ were dropwise added to the support. After impregnation, the precursors were dried at 383 K for 12 h and calcined at 673 K for 5 h with a ramping rate of 4 K/min. The catalysts with different ratios of Co/Cu were identified with the analysis of ICP-MS (NexION 300X, Perkin Elmer). For comparison, Co and Cu alone catalysts (5.0 wt %) were also prepared as well. The as-prepared catalysts were as denoted as Co_5—Cu_x/SiO_2, while Co was kept with 5.0wt % and the weight percentage of Cu (x) varied from 1.25 to 10.0 wt %.

Characterization

TEM. TEM images were conducted on a JEOL JEM 2100 microscope operated at 100 kV. The prepared samples were ultrasonically dispersed in hexane solvent by ultrasonic treatment and then dried over a carbon film supported on a Cu grid. The average size of metal particles was calculated on the basis of 250–300 particles.

XRD. XRD patterns were obtained with a Rigaku diffractometer (D/MAX 2550 VB/PC) using CuK_α radiation ($\lambda = 1.540589$ Å). For comparison, Co and Cu alone catalysts were also examined under the same conditions. Except for the detection of calcined catalysts, *in situ* XRD was performed for determining the active phase evolution in the temperature range 298–673 K in a mixture of H_2/He. The crystal size of metal particles was calculated with the width of diffraction patterns, referring to the full width of half maximum (FWHM) of crystalline facets at (111) for Cu or Co, (311) and (220) for Co_3O_4, (311) and (440) for $Cu_1Co_2O_4$ using debye-scherrer formula (Eq. 1)

$$D = \frac{0.9\lambda}{\Delta \cos\theta} \tag{1}$$

where D: crystal size, λ: wavelength of X-rays, Δ: FWHM of diffraction peak, and θ: angle corresponding to the peak.

TPR. Prior to the experiment, the sample (50 mg) was purged with Ar at 373 K in a flow rate of 30 mL/min for 2 h so that most of physical adsorbed H_2O could be removed from the samples. The TPR experiments were performed using a microfixed-bed reactor connected a thermal conducted detector (TCD). The temperature ramped from 303 to 1073 K with a ramping rate of 10 K/min in a 10% H_2/Ar flow (30 mL/min). The quantitative H_2 consumption was also evaluated for each sample.

N_2 Adsorption–Desorption. N_2 Adsorption and desorption isotherms were collected on an Autosorb-6 at 75 K. Prior to the measurements, the sample was degassed at 573 K until a stable vacuum of about 0.67 Pa was reached.

Kinetic measurement

Catalytic performance and kinetic measurements were carried out under differential conditions in a stainless steel continuous fixed-bed microreactor with a length of 450 mm, an inner diameter of 5 mm, and an external diameter of 8 mm, respectively (the flow chart of fixed-bed reactor [Supporting Information, Figure S1] system was depicted in Supporting Information). Three mass flow controllers were used to adjust automatically the flow rate of the inlet gases (H_2 (5.0), N_2(5.0), and syngas with different CO/H_2 ratios, Shanghai WOGE Gas Equipment). After reaching the specified temperature through a preheater, the gas flowed into the reactor, which was placed inside a tubular furnace capable of producing temperature up to 1073 K and controlled by a digital programmable controller. The reaction temperature was monitored by a thermocouple inserted into the catalyst bed with filling 200 mg catalyst, which was situated in the middle of the reactor. A back pressure regulator controlled the reaction pressure in the range 0.1–10.0 MPa. High-purity reaction gases (CO (4.5), H_2 (5.0), and N_2 (5.0)) were used. The conversion of CO (p_{CO}:0.375–3.0 MPa) was kept below

10.0%. Reactions were carried out in a temperature range 503–563 K in two different atmospheres: 1.5 MPa H_2, 0.375–3.0 MPa CO, rest N_2; 0.9 MPa CO, 0.45–3.6 MPa H_2, rest N_2. The external/internal diffusion effects can be ruled out following the procedures introduced by several previous studies.[34–36] The methods in detail were described in Supporting Information.

The catalyst was reduced *in situ* in a H_2 flow (0.6 MPa, 20 mL/min) at 673 K for 2 h. After reduction, catalysts were tested at specified temperature in a syngas flow (5.0 MPa) with desired ratios of H_2/CO. The blank test was carried out using SiO_2, and less than 0.1% conversion of CO was detected under reaction conditions (30% CO, 60% H_2, and 10%N_2, 5.0 MPa, GHSV 3500 h^{-1}, 543 K). This fact excluded the possible effects from the reactor wall and SiO_2.

Influent and effluent gases were analyzed with an online gas chromatography (Shanghai Ruimin GC2060). A capillary column (HP-Plot Al_2O_3/S) connected to a flame ionization detector (FID) was used to analyze hydrocarbon products. Other gases were determined using two packed columns (TDX-01 and 5A molecular sieve) connected to a thermal conductivity detector (TCD). Alcohols (C1—C5) and other oxygenates were analyzed off-line by another gas chromatograph with a capillary column free fatty acid phase (FFAP) connected to a FID using Ar as carrier gas after collected in a condenser. The oven temperature was held at 323 K for 3 min and then ramped up to 473 K at 30 K/min, and at which was maintained for 3 min. All the experimental data were obtained after reaction 20 h. The detailed analytic method for processing GC data can be seen in Supporting Information, while all absolute response factors for the chemicals in this system were measured (Supporting Information, Table S1 and S2).

Calculations

Absolute reaction rate of CO (r_{CO}) hydrogenation is expressed as Eq. 2

$$r_{CO} = \frac{v_{CO} \cdot X_{CO} \cdot Q_{in}}{m_{Me}} \quad [\text{mol s}^{-1}\text{g}_{Me}{}^{-1}] \tag{2}$$

m_{Me}–mass of Co in the reactor bed.

Q_{in}–total molar flow rate.

X_{CO}–CO conversion based on the product formation.

v_{CO}–concentration of CO in gas mixture, equal to p_i/p_0, p_i:partial pressure of reactants, p_0:total pressure in the system.

CO conversion (X_{CO}) was determined from summation of carbon number in all products (Eq. 3)

$$X_{CO}(\%) = \frac{Q_{out} \sum v_{gi} C_{gi} \cdot 20 \cdot 60/22400 + \sum m_{lj} C_{lj}/M_{lj}}{Q_{in} v_{CO} \cdot 20 \cdot 60/22400} \cdot 100\% \tag{3}$$

The selectivity for each product was obtained by Eqs. 4 and 5

$$S_{gi}(\%) = \frac{Q_{out} v_{gi} C_{gi} \cdot 100}{Q_{in} v_{CO} X_{CO}(\%)} \cdot 100\% \tag{4}$$

$$S_{lj}(\%) = \frac{m_{lj} C_{lj}/M_{lj} \cdot 100}{Q_{in} v_{CO} X_{CO}(\%) \cdot 20 \cdot 60/22400} \cdot 100\% \tag{5}$$

Space time yield of C2—C5 alcohols were calculated through Eq. 6

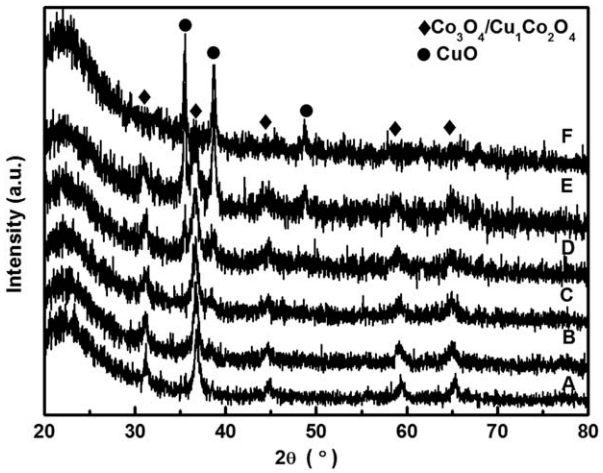

Figure 1. XRD patterns of unreduced CoCu/SiO_2 catalysts with different Co/Cu ratios.

(a) Co_5/SiO_2; (b) Co_5—$Cu_{1.25}/SiO_2$; (c) Co_5—$Cu_{2.5}/SiO_2$; (d) Co_5—Cu_5/SiO_2; (e) Co_5—Cu_{10}/SiO_2; and (f) Cu_5/SiO_2.

$$\text{STY}\,(\text{g}\cdot\text{kg}_{\text{cat}}^{-1}\cdot\text{h}^{-1}) = \frac{\sum_{j=2}^{5} m_{lj} C_{lj}/M_{lj}}{m_{cat}\, t} \tag{6}$$

Here, Q_{out} is the flow rate of the outlet gases, which equals the flow rate of the outlet gases Q_{in} at CO conversion of less than about 10%. v_{gi} is the volume fraction of i component in outlet gaseous products. C_{gi} is the carbon number of i component. m_{lj} is the mass of j component in liquid products. C_{lj} is the carbon number of j component. M_{lj} is the molar mass of j component. v_{CO} is the volume fraction of CO in inlet gases.

The rate in turnover frequency (TOF) (r_{TOF}, s^{-1}) was calculated following Eq. 7

$$r_{TOF} = \frac{r_{CO} M_{Co}}{d_{Co}} \times 100\% \quad [\text{s}^{-1}] \tag{7}$$

where M_{Co}: molecular weight of Co and d_{Co}: dispersion of Co. Here, we assume Co atoms play the role of active sites and all Co atoms were reduced to metallic states during reaction. Dispersion of Co atoms was calculated on the basis of spherical model.[37] For instance, a mean size of metallic Co particles over the fresh Co_5—$Cu_{2.5}/SiO_2$ catalyst was estimated to be about 10.6 nm (from XRD pattern), corresponding to a dispersion of 10.4%.

Results

Catalyst structure

XRD patterns of calcined catalysts in Figure 1 showed that Co_3O_4 was the primary oxide crystals for the Co alone catalyst, indicated by the plane facets (311) at 36.8°, (440) at 65.2°, (511) at 59.3°, and (220) at 31.2°. With keeping the same loading amount of Co (5.0 wt %) while increasing the Cu content from 1.25 to 10.0 wt %, the peak intensity for the CuO plane facets ($11\bar{1}$) at 35.5°, (111) at 38.7° increased steadily. In the meantime, the peaks for Co_3O_4 in the case of (311) shifted slightly from 36.8° to 36.7°, reflecting the possible expansion of Co_3O_4 lattice by interaction with Cu, and the lattice parameter d increased from 2.437 Å (Co_3O_4) to 2.444 Å (Co_5—Cu_{10}/SiO_2). As Cu cannot dissolve into the bulk Co to form Co—Cu alloy,[29] we assume only a few Cu

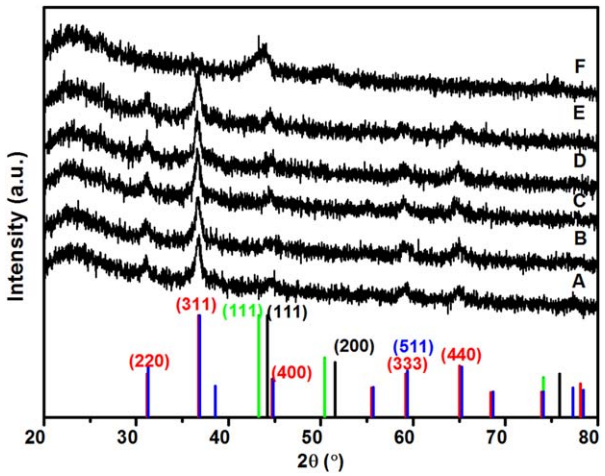

Figure 2. *In situ* XRD patterns of Co_5—$Cu_{2.5}/SiO_2$ during reduction process in 2%H_2/He at (a) 298 K; (b) 373 K; (c) 473 K; (d) 573 K; (e) 623 K; and (f) 673 K.

In reference spectra: $CuCo_2O_4$ (red), Co_3O_4 (blue), Cu (green), and Co (black). [Color figure can be viewed in the online issue, which is available at wileyonlinelibrary.com.]

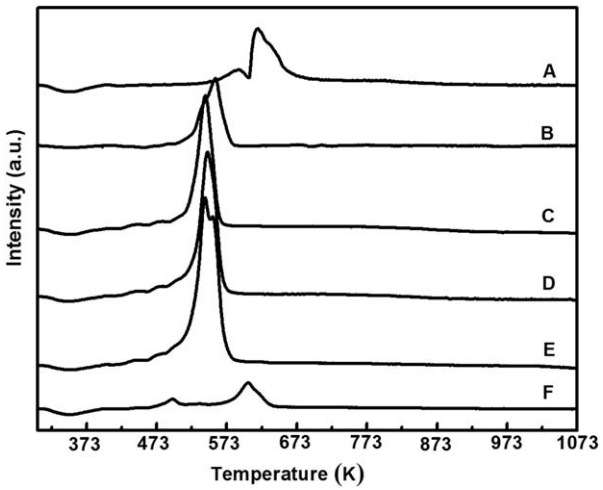

Figure 3. TPR profiles of $CoCu/SiO_2$ catalysts with different Co/Cu ratios in 10%H_2/Ar, ramping at 10 K/min.

(a) Co_5/SiO_2; (b) Co_5—$Cu_{1.25}/SiO_2$; (c) Co_5—$Cu_{2.5}/SiO_2$; (d) Co_5—Cu_5/SiO_2; (e) Co_5—Cu_{10}/SiO_2; and (f) Cu_5/SiO_2.

atoms penetrate into the bulk Co oxide. It is noted here that the most diffraction peaks for Co_3O_4 and $CuCo_2O_4$ were overlapped (see the bottom reference spectra in Figure 1), so it is difficult to distinguish the two components in this system.

To determine the changes in catalyst structure during the activation (pretreatment) process, *in situ* XRD patterns for the Co_5—$Cu_{2.5}/SiO_2$ catalyst were recorded in a stream of H_2 (3%H_2/He, 15 mL/min) from 298 to 673 K (Figure 2). It can be seen that from 298 to 623 K, Co_3O_4 was slightly reduced with referencing the intensity for Co_3O_4 (311) at 36.7°, while the peaks for CuO were not clearly observed. With further raising the temperature to 673 K, the peak at 36.7° disappeared completely while a new broad peak at 44.5° between Co(111) at 44.2° and Cu(111) at 43.3° was observed, possibly corresponding to bimetallic CoCu (111). By taking a close look, there is still some unreduced Co_3O_4 as indicated by the small peak at 36.7° in Figure 2f. In a similar experiment, Smith et al.[38] also observed the transformation from Co_3O_4 to Co^0 in the temperature range 573–673 K in a system of CoCu.

For the further investigation of the interaction between both Co_3O_4 and CuO during activation process, H_2-TPR experiments were performed over single and bimetallic catalysts (Figure 3). There were two reduction peaks at 588 K (weak) and 618 K (strong) observed for the Co alone catalyst (profile A in Figure 3); while two peaks at 495 K (weak) and 602 K (stong) could be detected for the Cu alone catalyst (profile F in Figure 3). With introduction of Cu from 1.25 to 10.0 wt %, only one peak could be seen in the whole temperature range, while the peak position shifted down from 618 to 546 K, companying with an increase in intensity. The quantitative H_2 consumption during TPR was listed in Table 1.

Table 1. Quantitative H_2 Consumption During TPR

Catalyst	H_2 Consumption (mmol/g)	Expected H_2 Consumption[a] (mmol/g)	Expected H_2 Consumption[b] (mmol/g)
Co_5/SiO_2	1.26	1.13	1.13
Co_5—$Cu_{1.25}/SiO_2$	1.50	1.33	1.39
Co_5—$Cu_{2.5}/SiO_2$	1.76	1.52	1.65
Co_5—Cu_5/SiO_2	2.34	1.92	2.06
Co_5—Cu_{10}/SiO_2	2.91	2.70	2.85
Cu_5/SiO_2	0.78	0.79	0.79

[a]Assuming complete conversion of CuO and Co_3O_4 to Cu^0 and Co^0, respectively.
[b]Assuming $Cu_1Co_2O_4$ spinel structure exist in $CuCo/SiO_2$ catalysts prior to CuO and Co_3O_4.

Following the same pretreatment procedure in Figure 2, the fresh reduced Co_5—$Cu_{2.5}/SiO_2$ catalyst was measured using a high-resolution TEM (Figure 4a). The metallic particles were randomly distributed in a range from 1.8 to 14.0 nm. In terms of the particle size, with considering the XRD results and the comparison of the TEM images, all metal particles can be roughly classified into two types through the TEM histogram analysis: (1) Larger particles from 4.0 to 14.0 nm with a mean size of 7.6 ± 2.2 nm (Figure 4b), which is consistent with the XRD analysis and (2) Smaller particles from 1.8 to 4.0 nm with an average particle size of 2.5 ± 0.4 nm, which are too small to be detected by XRD (Figure 4c) but visible in TEM images. Due to the technology limitations, the composition of those particles is difficult to be identified. It is noted that a twin particles consisting of Co and Cu could be observed in Figure 4a, the boundary between Co and Cu and its role in this reaction needs further study.

CO hydrogenation over CoCu catalysts with different Co/Cu ratios

CO hydrogenation was performed over catalysts with different Co/Cu ratios, while the distributions of all products were outlined in Table 2. Among all catalysts, the highest CO conversion was observed for Co_5/SiO_2 while the primary products were hydrocarbons; this agrees with the fact that metallic Co^0 is the active component of F–T catalysts.[39] Conversely, Cu is the active component of methanol synthesis catalysts,[40] which can activate and hydrogenate CO molecule into methanol (the selectivity of ~40%). However, the

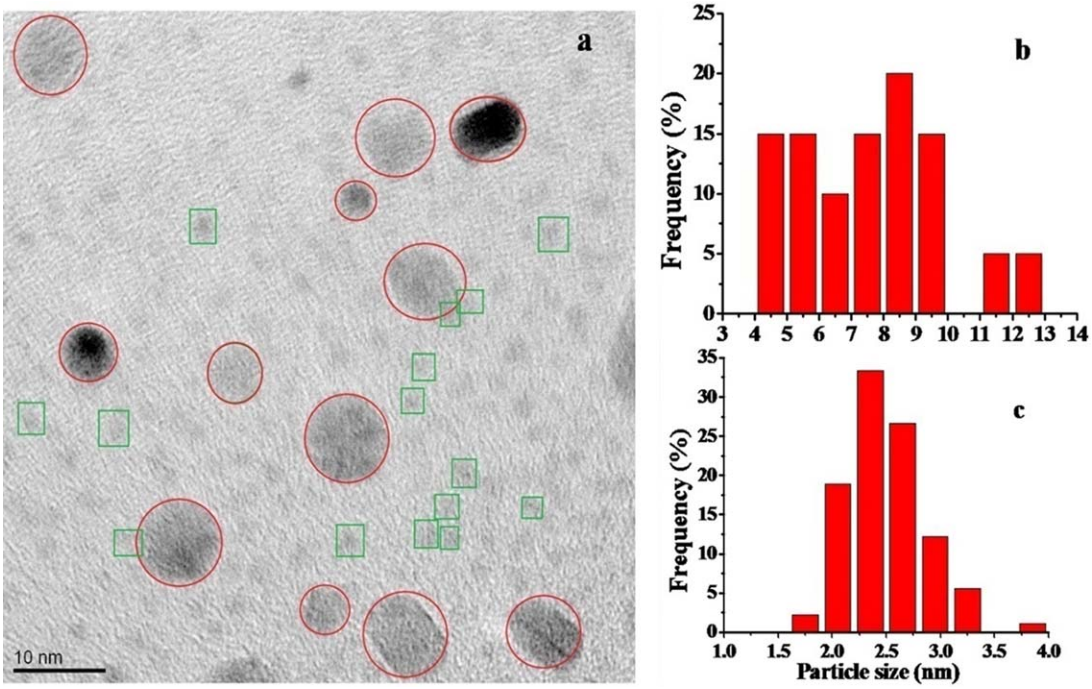

Figure 4. TEM image (a) and histogram analysis of larger particles from 4.0 to 14.0 nm (b) and smaller particles from 1.8 to 4.0 nm (c) over a fresh reduced Co_5—$Cu_{2.5}/SiO_2$ catalyst.

Circle (larger particles) and square (smaller particles). [Color figure can be viewed in the online issue, which is available at wileyonlinelibrary.com.]

single Cu catalysts showed extremely low activity, lower than that for Co by about two magnitudes. Therefore, in the present system Co^0 is regarded as the main active metal.

The reaction rates for bimetallic CoCu catalysts demonstrated the reactivity of Co was decreased remarkably with the rise of Cu content. The primary gaseous products over bimetallic CoCu catalysts were linear hydrocarbons and the collected liquid products mainly consisted of C_1—C_5 linear alcohols. In the meantime, the selectivity toward higher alcohols was greatly enhanced with the addition of Cu. It is noted that the selectivity to C_2—C_5 alcohols was increased from 1.82% (Co_5/SiO_2 at lower CO conversion of 2.30%) to 3.54% with the addition of 1.25 wt % Cu, and surpassed a maximum selectivity of 4.15% with 2.5 wt % Cu, and then went down to 3.90% with continuous addition of Cu to 10.0 wt %. The widely accepted reaction mechanism of HAS involves CO dissociation (C_{dis}) and CO associative insertion (C_{ins}).[41,42] To describe the effect of Cu/Co ratio on catalytic performance, selectivity descriptors ($\Phi = C_{ins}/C_{dis}$) defined by Prieto et al.[43] were calculated and shown in Table 2. As observed, the Φ value for Cu alone catalyst (Cu_5/SiO_2) was as high as 0.67, indicating that Cu preferred CO associative insertion, while a much lower value of 0.039 for Co alone catalyst (Co_5/SiO_2) revealed that Co was in favor of CO dissociation. However, for these bimetallic catalysts, the Φ values did not show a proportional correlation with the change of Cu/Co ratio. It first went up until a maximum value of 0.089 (Co_5—$Cu_{2.5}/SiO_2$) was reached, then monotonously dropped down to 0.081 (Co_5—Cu_{10}/SiO_2). This relation illustrates that CO associative insertion and CO dissociation could not be attributed to the simple overlap of individual Cu atoms and Co atoms. In other words, the interaction between Cu and Co plays a significant effect on Φ value and selectivity of high alcohols. The detailed explanations to this phenomenon will be discussed later. Likely, for HAS, the optimum composition of the catalyst contains 5 wt % Co and 2.5 wt % Cu, which was selected for the proceeding kinetic study. It is noted that on the basis of XRD patterns, the size of Co particles in the Co_5—$Cu_{2.5}/SiO_2$ catalyst was estimated to be 10.0 nm, corresponding to a dispersion of 10%. Assuming that the metal particle size remains unchanged during reaction, the rate in TOF should be 3.0×10^{-2} s^{-1} according to the mass-based rate in Table 2. In addition, the selectivity to CO_2 was very low (~2%) for all catalysts, which means Co-based catalysts had low activity for the water-gas shift reaction, consistent with previous works from other groups.[44]

Kinetics

Internal and External Diffusion Effects. The external diffusion effects were excluded through varying the boundary layer thickness of the catalyst external surface, which was obtained by changing gas hourly space velocity (GHSV).[45] The reaction was carried out at 543 K, 5.0 MPa of syngas with a H_2/CO ratio of 2, catalyst particle size of 0.177 mm and GHSV = 3450, 10350, and 14900 h^{-1}, respectively. Figure 5a reveals that CO conversion decreased from 11.9 to 3.1% with increasing GHSV from 3450 to 14,900 h^{-1}. The corresponding mass-transfer coefficient (k_c) was calculated and summarized in Supporting Information, Table S3. It is clear that the effect of flow rate on the external diffusion is negligible at above the GHSV of 10,350 h^{-1}. Therefore, we conclude that the external mass transport effects can be safely precluded at the GHSV of 14,900 h^{-1}.

Conversely, the internal diffusion effects were phased out by changing the catalyst particle size.[41] The catalysts with different particle sizes (0.125–0.147, 0.147–0.177, 0.177–0.25, and 0.25–0.42 mm) were examined at 543 K, 5.0 MPa

Table 2. Effects of Different Cu—Co Ratios on Activity and Selectivity of all Products[a]

Catalysts	Conv. (%)	Selectivity, Carbon Based (%)											STY ($g\ kg_{cat}^{-1}\ h^{-1}$)	$r_{CO}/10^{-5}$ ($mol\ g_{Co}^{-1}\ s^{-1}$)
		CH_4	C_2H_n	C_3H_n	C_4H_n	HC_S	CH_3OH	C_2H_5OH	C_3H_7OH	C_4H_9OH	C_2—C_5OH	ROH	CO_2	Φ[b]		
Co_5/SiO_2	11.75	50.90	7.76	13.26	4.73	92.41	3.84	0.87	0.38	0.24	1.60	5.44	2.03	0.039	18.15	27.70
Co_5—$Cu_{1.25}/SiO_2$	2.42	44.27	10.71	16.04	3.85	87.73	6.52	2.17	1.07	0.29	3.54	10.05	1.73	0.074	8.47	5.74
Co_5—$Cu_{2.5}/SiO_2$	2.03	45.39	10.13	15.11	3.71	85.52	7.74	2.44	1.24	0.46	4.15	11.88	2.14	0.089	8.28	4.80
Co_5—Cu_5/SiO_2	1.63	44.78	10.35	15.71	3.99	85.97	7.30	2.22	1.20	0.41	3.97	11.27	2.30	0.083	6.30	3.83
Co_5—Cu_{10}/SiO_2	1.37	43.59	10.02	15.46	4.10	85.85	7.16	2.16	1.14	0.40	3.90	11.06	2.27	0.082	5.21	3.23
Cu_5/SiO_2	0.05	25.97	15.73	9.47	3.81	57.41	38.05	0.87	–	–	0.87	38.93	3.10	0.665	0.04	–
Co_5/SiO_2[c]	2.30	49.64	6.03	12.02	8.80	91.19	4.44	1.01	0.47	0.23	1.82	6.26	2.10	0.046	20.02	27.72

[a]Reaction conditions: 200 mg catalysts, $P = 5.0$ MPa, $T = 533$ K, Reaction time = 20 h, $H_2/CO/N_2 = 6/3/1$, GHSV = 14,900 h^{-1}.
[b]Selectivity descriptor ($\Phi = C_{ins}/C_{dis}$), which defined by Prieto et al.[43]
[c]Reaction conditions: 40 mg catalysts diluted in 160 mg SiO_2, $P = 5.0$ MPa, $T = 533$ K, Reaction time = 20 h, $H_2/CO/N_2 = 6/3/1$, GHSV = 14,900 h^{-1}.

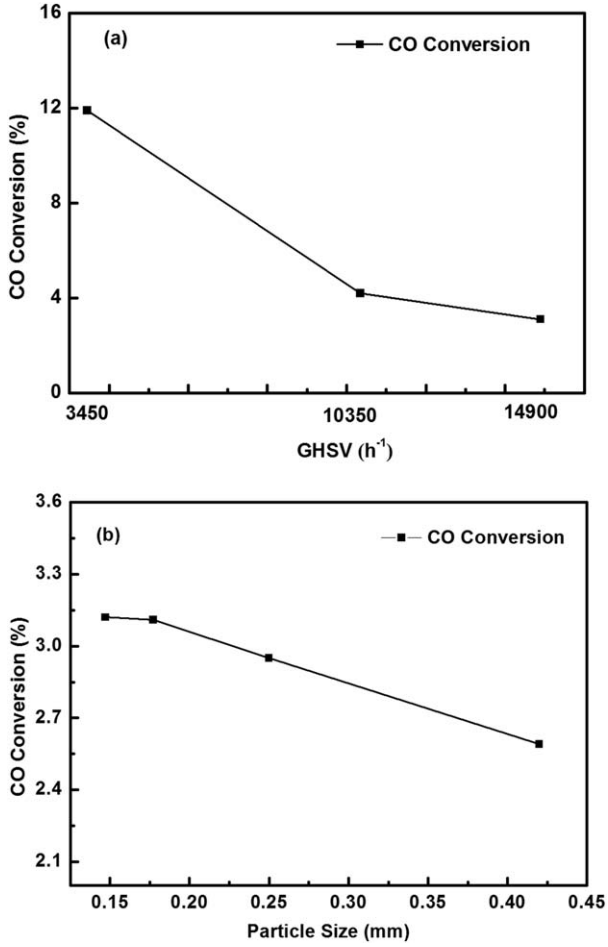

Figure 5. (a) Dependence of CO conversion on GHSV over a Co_5—$Cu_{2.5}/SiO_2$ catalyst (0.177 mm) at 543 K, 5.0 MPa, $H_2/CO/N_2 = 6/3/1$ and (b) dependence of CO conversion on a Co_5—$Cu_{2.5}/SiO_2$ catalyst with a size of 0.42, 0.25, 0.177, and 0.147 mm, respectively, at 543 K, 5.0 MPa, $CO/H_2 = 1$, GHSV of 3500 h^{-1}.

of syngas with a GHSV of 14,900 h^{-1} and H_2/CO ratio of 2. The results in Figure 5b revealed that CO conversion increased linearly with a decrease in the catalyst particle size at 0.177–0.42 mm, and became constant when the particle size was smaller than 0.177 mm. The Weisz-Pratercriterion (C_{WP}) is usually used to estimate the internal mass-transfer resistance in heterogeneous catalytic reactions.[36] If $C_{WP} << 1$, there is no internal diffusion limitation, and if $C_{WP} >> 1$, internal diffusion has an effect on the reaction. The value of C_{WP} of 0.082 was calculated for the catalysts with an average particle diameter of 0.177 mm, indicating that the internal diffusion could be negligible. More details have been described in Supporting Information.

Kinetics Measurements for HAS. Ahead of kinetic measurements, the stability of catalyst (Figure 6) was examined under standard reaction conditions. It can be seen that CO conversion and CH_4 formation remained unchanged after 45 h time-on-stream. It is an indicative that the active sites for HAS were unlikely altered during the reaction.

The power-law function was applied for fitting the kinetic data (Eq. 8). The parameters include apparent activation

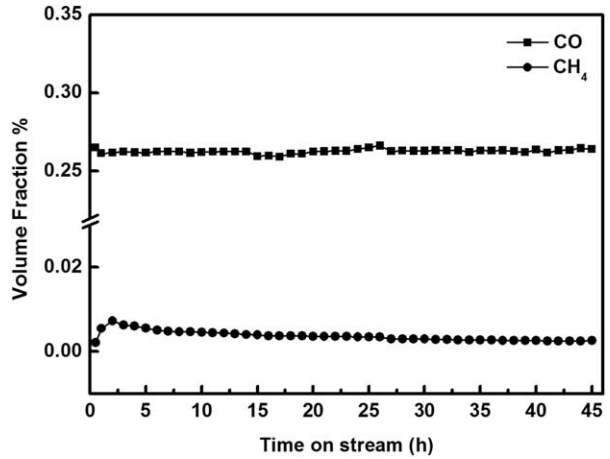

Figure 6. Catalytic stability for HAS over a Co_5—$Cu_{2.5}$/SiO_2 catalyst (0.177 mm).

Reaction conditions: 5.0 MPa, $H_2/CO/N_2 = 6/3/1$, GHSV = 14,900 h^{-1}, 543 K.

energies (E_a) and reaction orders with respect to CO (β) and H_2 (γ), which can reflect the effects of reaction temperature and reactant partial pressure directly on the rate. In addition, the simple model also has an important guiding significance in the process of reactor scaling-up

$$r_A = k * P_{CO}^{\beta} * P_{H_2}^{\gamma} \tag{8}$$

The dependence of reaction rates with respect to CO partial pressure ($p_{H_2} = 1.5$ MPa and $p_{CO} = 0.375$–3.0 MPa) and H_2 partial pressure ($p_{CO} = 0.9$ MPa and $p_{H_2} = 0.45$–3.6 MPa) at 513, 533, and 553 K were illustrated in Figure 7 on the basis of the yields for all products, respectively. It can be observed that the reaction rates based on the formation of different hydrocarbons, such as CH_4 (Figures 7a, b), C_2H_n (Figures 7c, d), and C_3H_n (Figures 7e, f), were increased with the rise of temperature at 513–553 K. In the meantime, the reaction rates for the formation of CH_4 and C_2H_n were reduced with an increase inp_{CO}, but dependent onp_{H_2}. For the formation of C_3H_n, the same phenomenon was observed at 513 and 533 K. We noticed that the reaction behavior toward C_3H_n formation was slightly changed at 553 K, and the reaction rates were almost independent onp_{CO} orp_{H_2}. Under the same reaction conditions, the formation rates of alcohols, such as CH_3OH (Figures 7g, h) and C_2H_5OH (Figures 7i, j), vs.p_{CO} or p_{H_2}, were also depicted. Similar relationships, the rates going down with the rise of p_{CO} and up with p_{H_2}, were observed in the whole temperature range. However, the formation rates increased at 513–533 K, but almost remained unchanged at 533–553 K, even by changing the CO/H_2 ratio in feedgas.

The rate constant can be expressed as Eq. 9

$$k = k_0 * \mathrm{Exp}\,(-E_a/\mathrm{RT}) \tag{9}$$

The dependency of the formation rates for alcohols (Figure 8a) and hydrocarbons (Figure 8b) on the reciprocal of the reaction temperature at 503–563 K (the Arrhenius plots) was illustrated. All kinetic parameters, including reaction orders and apparent activation energies, were summarized in Table 3. The E_a of 124.9, 122.8, and 117.6 kJ mol^{-1} were determined for CH_4, C_2H_n, and C_3H_n, respectively. Only a small difference in E_a values indicates that the distribution of hydrocarbons is not sensitive to the reaction temperature at 503–563 K. In comparison, the E_a value for alcohols is much lower than that for hydrocarbons, about 53.5 kJ mol^{-1} for CH_3OH and 70.0 kJ mol^{-1} for C_2H_5OH. That means the reduction of reaction temperature is favorable for HAS as mentioned in previous studies.[46,47]

Chain growth is a key step in HAS, and the distribution of alcohols could be described by the Anderson–Schulz–Flory equation (Eqs. 10 and 11) as it is usually used in F–T synthesis[20,42]

$$W_n = n \cdot \alpha^{n-1}(1-\alpha)^2 \tag{10}$$

$$\ln\left(\frac{W_n}{n}\right) = n \cdot \ln\alpha + 2\ln\left(\frac{1-\alpha}{\sqrt{\alpha}}\right) \tag{11}$$

As listed in Table 4, the chain growth probability for alcohols was almost unchanged in the temperature range 513–533 K, but decreased at 553 K, again, which suggests that HAS is unfavorable with the rise of temperature.

Discussion

Based on the above mentioned results, it is clear that the addition of Cu into Co greatly promoted the selectivity toward HAS, but lowered the catalytic activity. The kinetic behaviors and the product distributions have been investigated on bimetallic CoCu catalysts. Therefore, in this section, the discussion will be focused on two aspects: (1) the Co structural modification by interaction with Cu, and its effects on the catalyst performance and (2) the distribution of products, especially higher alcohols, over a bimetallic CoCu catalyst, and plausible mechanisms for HAS on the basis of kinetics. It is noted that Co is regarded as the primary active metal in this system; however, the conversion of syngas over the single Co catalyst, as a F–T catalyst,[48–51] and over the single Cu,[52,53] as a methanol synthesis catalyst, will not be mentioned here, because they have already long been studied.

Interaction of Co and Cu

It has proved that bulk Cu and Co unlikely form alloy because two metals have low solubility into each other.[29] In this study, nanoscale metal particles were produced as identified by TEM images (Figure 4). *In situ* XRD patterns in Figure 2 demonstrated that there were diffraction peaks possibly responsible for bimetallic CoCu phase (CoCu nanosized alloys) during reduction process. Furthermore, TPR profiles (Figure 3) revealed that the interaction between Co and Cu did exist as indicated by the remarkable downshifts of the reduction peaks, which is an indicative for the enhanced reducibility of CoCu catalysts.[21,54] The presence of Cu facilitates the reduction of Co oxides, especially in nanoscale Co particles, as evidenced by Carenco et al.[31] using ambient-pressure X-ray photoelectron spectroscopy and high-pressure X-ray absorption spectroscopy. Several previous studies[29,55–58] have also suggested that nanoscale alloying of Cu and Co could happen and be responsible for the enhanced selectivity to higher alcohols.

In theory, the CoCu nanoalloy surfaces should be enriched with Cu because the surface energy of Cu(1.934 J m^{-2}) is lower than that of Co(2.709 J m^{-2}).[59] However, it was found that dealloying of Co from CoCu nanoparticles, or to say, segregation, might occur under syngas exposure by forming Co-rich (majority morphology) and Cu-rich (minority

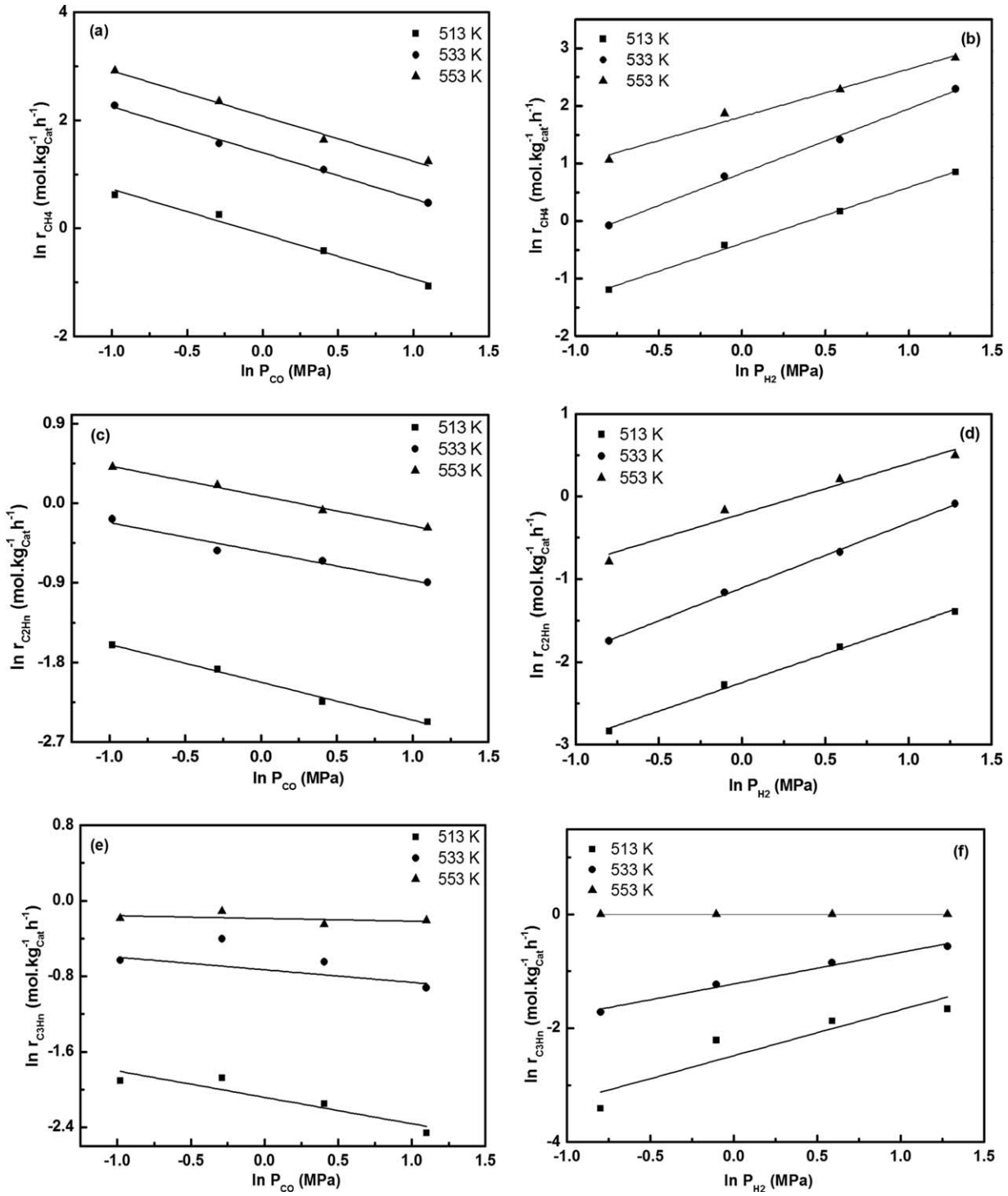

Figure 7. Dependence of formation rate on partial pressure of CO(left) and H_2(right).

(a, b) CH_4; (c, d) C_2H_n; (e, f) C_3H_n; (g, h) CH_3OH; and (i, j) C_2H_5OH.

morphology) nanoparticles.[31] Individual particles in the fresh reduced catalyst were also visible in our TEM images in Figure 4. Unfortunately, the contemporary techniques are still unable to follow up the structural changes of catalysts under the realistic HAS conditions, especially when the reductant is the high-pressure syngas instead of H_2. Studies on single crystal surfaces,[60] supported catalysts[39,61] and density functional theory calculations[62] have revealed that Co surfaces could undergo a surface reconstructure upon exposure to F–T conditions. The spectroscopic study for the determination of catalyst structure during HAS by this group (Operando study) will be published elsewhere.

Compared with the activity of the Co alone catalyst, under the same reactions the activity contributed by single Cu particles can be negligible over CoCu catalysts. As a result, if the Co surface is enriched with Cu, the active sites for CO dissociation, which has proved mainly to occur on Co ensembles, was reduced with a decrease in the surface Co

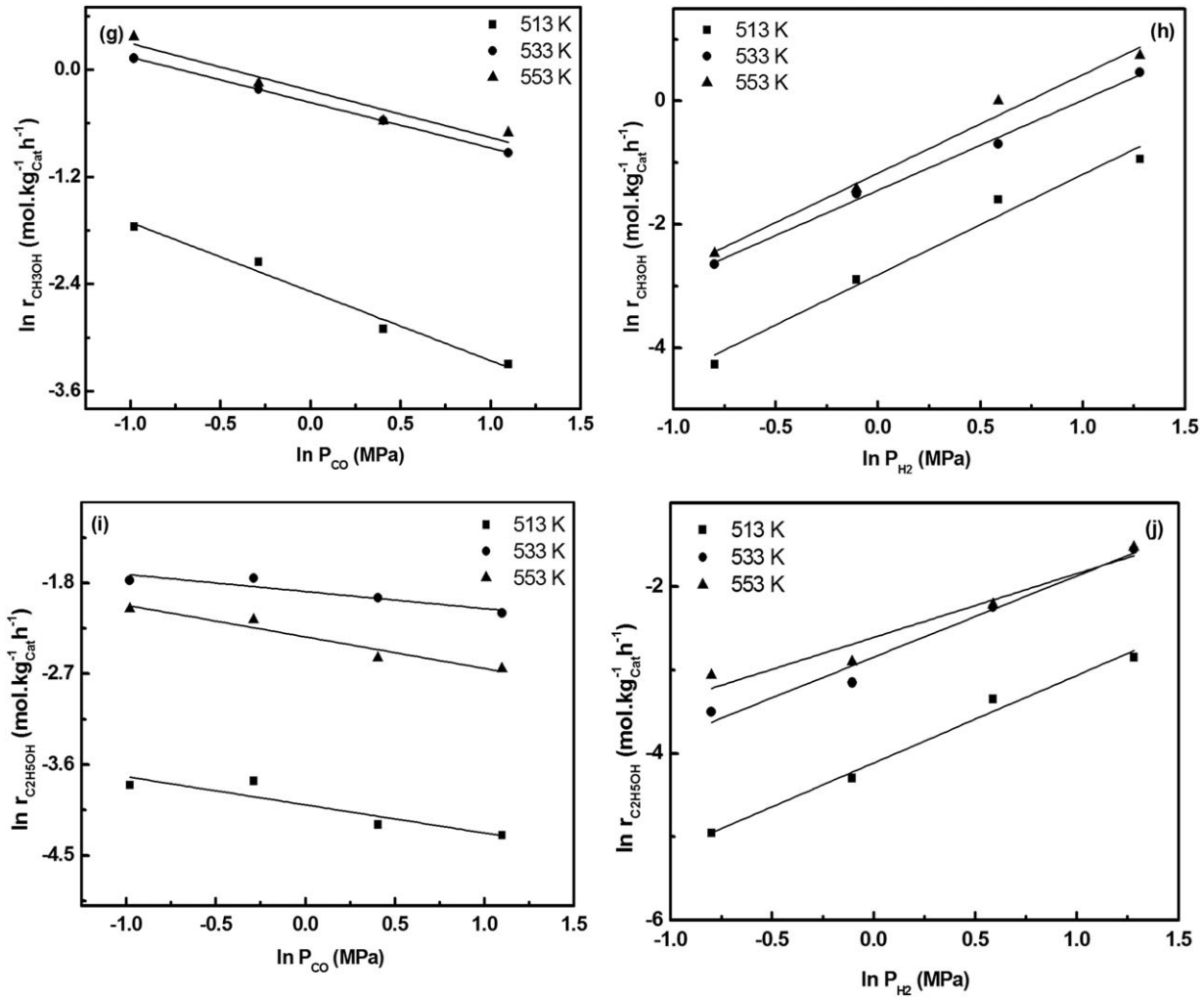

Figure 7. (Continued)

atoms, thus leading to a drop in the reaction rate by a factor of 10 (Table 2). Jacobs et al.[54] also found that the increased fraction of reduced Co did not translate to improved active site intensity. It is noted that during the reaction CO-induced migration of metallic atoms could not be excluded. For instance, it is reported that CO binds relatively weakly to Cu surfaces (46–59 kJ/mol),[63] while more strongly to Co surfaces (140 kJ/mol for Co (110)).[64] The reactant-induced structural change or redistribution of Cu and Co atoms is still a great challenge in this study.

In addition, Smith et al. revealed that addition of Cu could increase the reducibility of $Co_3O_4 \rightarrow CoO$; while the addition of Co to Cu/SiO_2 could also result in the formation of an amorphous CuO that was more easily reducible than crystalline CuO[38] and prevent the formation of less reducible Cu_2O species. This explained well that the position of the primary reduction peaks for bimetallic CoCu catalysts in TPR profiles, compared with those for both single Co and Cu catalysts, remarkably shifted down (Figure 3) from 618 K (Co) and 602 K (Cu) to about 546 K (CoCu). Up to now, most of experimental evidences and theoretical calculations[65–67] suggest that the metallic Co^0 should be the active sites for HAS, because it is easy to form CoC_x during the reaction, which is the so-called "active species" for HAS. However, Co^0 may not be stable during the reaction and could be probably oxidized by the O* from CO dissociation and H_2O from H_2 oxidation. Further discussion about this issue is beyond this study.

Plausible mechanism for HAS

It is well known that Co-based catalysts have already been adopted by industry as the F–T process catalysts, which is a surface-catalyzed polymerization process.[68] CH_x monomers, yielded by the dissociation and hydrogenation of adsorbed CO, are the building blocks for the subsequent chain growth reactions to produce hydrocarbons, olefins, alcohols, oxygenates, and wax. Many works have been contributed to the rationalization of the mechanisms for the F–T process over Co-based catalysts.[69,70] The generally accepted pathways for syngas conversion were illustrated in Scheme 1,[24] which includes chain growth in F–T synthesis and some secondary reactions for olefin hydrogenation to paraffins, and hydrogenolysis or hydroformylation to alcohols. It has proved that for syngas conversion the reaction rate and selectivity to C2+ compounds over Co-based catalysts were affected by several factors, such as the size of metal crystallites,[71] the support property,[72–74] and the second metal.[75] In this study,

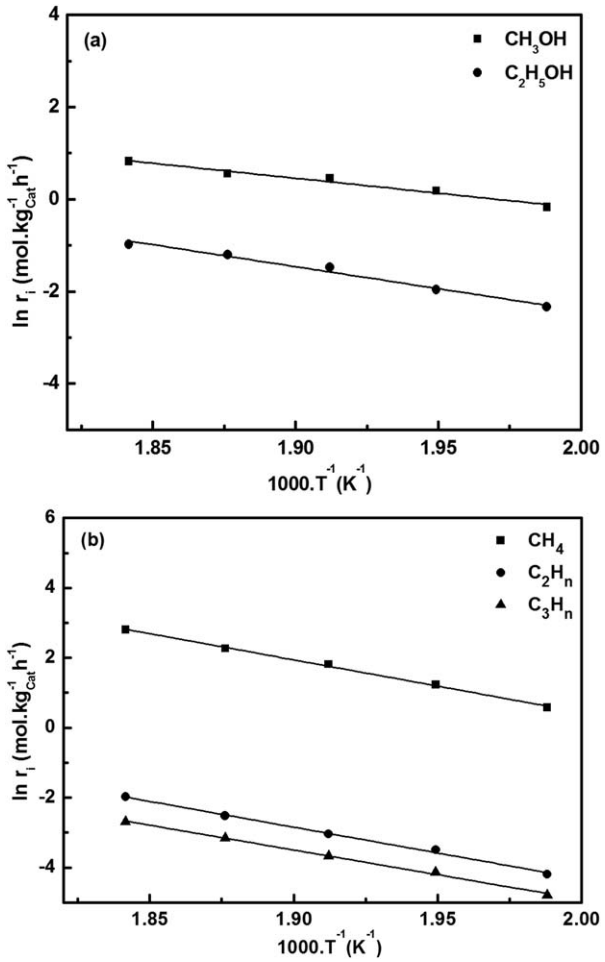

Figure 8. Arrhenius diagrams of products.

Reaction conditions: $P = 5.0$ MPa, $H_2/CO/N_2 = 6/3/1$, GHSV = 14,900 h^{-1}, $t = 20$ h, $T = 503$–543 K.

for the sake of brevity, we only discuss how the HAS reaction is affected by the addition of Cu to Co catalyst.

As listed in Table 2, compared with the single Co catalyst, the selectivities to C2+ compounds were significantly increased with the addition of Cu while a drop of 5% selectivity to CH_4 was observable. Likely, Cu in bimetallic CoCu catalysts can enhance CO insertion termination pathways that form alcohols and γ-hydrogen abstraction steps leading to internal olefins. As a result, the selectivity to C2—C5 alcohols was almost increased by a factor of two. Conversely, the remarkable drop in CO conversion was observed in the presence of Cu, indicating that Cu atoms may be adsorbed on high-energy Co sites, or so-called B5 sites which were identified to be favored for CO dissociation.[76–78]

The pressure-dependent reaction rates at different temperatures (Figure 7) and the kinetic parameters (Table 3) showed that the reaction orders with respect to H_2 for all products were usually positive; on the contrary, corresponding reaction orders with respect to CO were all negative, except for $\sim$0 order for CO and H_2 at 553 K for the formation of C_3H_n. Those reaction orders indicate that all reactions including HAS were proceeded through a Langmuir-Hinshelwood model, while CO and H_2 were dissociated and reacted on the solid catalyst surfaces. The negative order with respect to p_{CO} suggested that the catalyst surface was covered with the strong adsorbed CO or intermediate C* from CO dissociation, which may block the adsorption of H_2 or subsequent H_2 dissociation. $\sim$0 orders for CO and H_2 in the formation of C_3H_n at 553 K indicate that the formation rate for this species, or to say, the chain growth, is decided by intermediates, which is easily formed by adsorption of reactants or surface reactions.

Moreover, the rates for alcohol formation (Figures 7g, j) were less affected by temperature at 533–553 K than those at 513–533 K. Especially, when increasing the temperature from 533 to 553 K, the formation rates for C_2H_5OH were approaching by rising the H_2/CO ratio, almost to be identical at $p_{H_2} > 0.5$ MPa (Figure 7j). A similar result was also observable for CH_3OH formation (Figure 7h). Likely, alcohols might be easily transferred by hydrogenolysis in H_2-rich atmosphere at high temperatures. Conversely, the E_a for the formation of alcohols is about half of that for the formation of hydrocarbons, it is an evidence that Cu modified active Co sites favor the formation of alcohols, however, the role of Cu atoms is still unclear. In addition, the yield of hydrocarbons and alcohols decreases linearly with the increase of carbon chain length. Mo et al.[33] has proposed that Co atoms were highly dispersed with the addition of Cu, with few or no large ensembles ($n \geq 12$) existing on the catalyst surface, which may terminate the chain growth process.

Conclusions

A series of bimetallic CoCu nanoparticles on SiO_2 were prepared. XRD patterns demonstrated that Co_3O_4 and CuO existed on the catalyst surface as precursors; *in situ* XRD

Table 3. Apparent Activation Energies and Reaction Orders for Different Products

		Reaction Orders					
		513 K		533 K		553 K	
Products	Activation Energies (kJ mol^{-1})	H_2	CO	H_2	CO	H_2	CO
CH_4	124.93	0.97	−0.83	1.12	−0.85	0.83	−0.83
	±3.47	±0.04	±0.07	±0.05	±0.04	±0.08	±0.06
C_2H_n	122.79	0.69	−0.43	0.79	−0.33	0.61	−0.34
	±4.01	±0.03	±0.03	±0.02	±0.05	±0.08	±0.02
C_3H_n	117.63	0.81	−0.28	0.55	−0.16	∼0	∼0
	±3.13	±0.24	±0.08	±0.05	±0.12		
CH_3OH	53.90	1.63	−0.77	1.46	−0.51	1.60	−0.53
	±4.97	±0.17	±0.07	±0.07	±0.01	±0.13	0.09
C_2H_5OH	79.23	1.05	−0.28	0.97	−0.17	0.76	−0.31
	±5.75	±0.09	±0.09	±0.11	±0.05	±0.13	±0.05

Table 4. Chain Growth Probability for Alcohols at Different Temperatures[a]

T (K)	503	513	523	533	543	553	563
α	0.499	0.496	0.487	0.501	0.507	0.402	0.395

[a]Reaction conditions: $P = 5.0$ MPa, $H_2/CO/N_2 = 6/3/1$, GHSV = 14,900 h^{-1}, $t = 20$ h, catalyst: 200 mg, 0.177 mm.

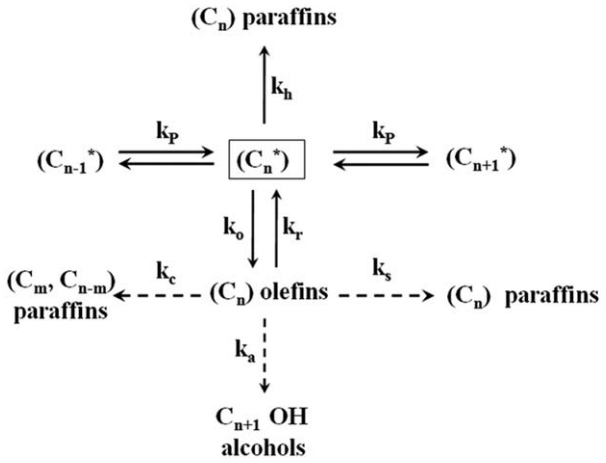

Scheme 1. Chain growth pathways and possible secondary reactions of olefins in the Fischer-Tropsch synthesis.

patterns have proved that there was no formation of CoCu alloys, and the metallic Co was formed at 673 K. Metal nanoparticles in the fresh reduced catalyst were highly dispersed as identified by High Resolution Transmission Electron Microscopy (HRTEM) images. The interaction between Co and Cu may exist as evidenced by downshifts of the reduction peaks in TPR profiles.

CO hydrogenation was assumed to occur mainly on Co sites. Cu modified Co catalysts (bimetallic CoCu) exhibited higher selectivity to HAS than the Co alone catalyst, while the activity to CO conversion was greatly decreased. Perhaps, the active Co sites were covered by Cu atoms, thus also leading to a decrease in the selectivity to CH_4. It was also evidenced that the distribution of products only changed moderately with varying the Co/Cu ratio.

The intrinsic kinetics of CO hydrogenation was measured over a Co_5—$Cu_{2.5}/SiO_2$ catalyst at temperature 513, 533, 553 K under a total pressure of 5.0 MPa. It was found that all reaction orders with respect to CO are negative and positive value to H_2 orders; while the E_a to the formation of alcohols is about half of that for hydrocarbons. Clearly, CO hydrogenation is proceeded through a Langmuir-Hinshelwood mechanism, while CO or the intermediate C* from CO dissociation blocks the adsorption of H_2 and its subsequent dissociation. In general, the HAS over bimetallic CoCu catalysts is favorable at low temperature; at above 533 K, H_2-rich atmosphere may convert alcohols by hydrogenolysis.

Acknowledgments

The authors are grateful to the support from the National Science Foundation (21176071, 21106041, 21273070), the Program for New Century Excellent Talents in university (NCET-12–0852), Science and Technology Commission of Shanghai Municipality (11JC1402700), Innovation Program of Shanghai Municipal Education Commission (11ZZ52, 12ZZ051), Shanghai Natural Science Foundation (11ZR1408400), Fundamental Research Funds for the Central Universities and the Chinese Education Ministry 111 project (B08021).

Literature Cited

1. Subramani V, Gangwal SK. A review of recent literature to search for an efficient catalytic process for the conversion of syngas to ethanol. *Energy Fuels*. 2008;22:814–839.
2. Rostrup-Nielsen JR. Fuels and energy for the future: the role of catalysis. *Catal Rev Sci Eng*. 2004;46:247–270.
3. Conti J, Holtberg P, Beamon JA, Napolitano S, Schaal AM, Turnyre JT, Westfall L, Doman LE. International Energy Outlook. Washington, DC: U.S. Department of Energy. Available at: www.eia.gov/oiaf/ieo/index.html. Accessed on 31 August 2013.
4. Fischer F, Tropsch H. The synthesis of petroleum at atmospheric pressures from gasification products of coal. *Brennst Chem*. 1926;7:97–104.
5. Dybkjr I, Christensen TS. Syngas for large scale conversion of natural gas to liquid fuels. *Stud Surf Sci Catal*. 2001;136:435–440.
6. Huber GW, Chheda J, Barrett CB, Dumesic JA. Production of liquid alkanes by aqueous-phase processing of biomass-derived carbohydrates. *Science*. 2005;308:1446–1450.
7. Petrus L, Noordermeer MA. Biomass to biofuels, a chemical perspective. *Green Chem*. 2006;8:861–867.
8. Steynberg A, Dry M. *Fischer-Tropsch Technology*. Amsterdam: Elsevier, 2004.
9. Entenberg RD, Menard AL. Future octane number requirements for future market demand. *J Mark*. 1966;30:28–32.
10. Marin A, Kodjak D, Brown D, Rao H. *Relative Cancer Risk of Reformulated Gasoline and Conventional Gasoline Sold in the Northeast*. Boston: Northeast States for Coordinated Air Use Management, 1998.
11. Surisetty VR, Dalai AK, Kozinski J. Alcohols as alternative fuels: an overview. *Appl Catal A*. 2011;404:1–11.
12. Mei D, Rousseau R, Kathmann SM, Glezakou VA, Engelhard MH, Jiang W, Wang C, Gerber MA, White JF, Stevens DJ. Ethanol synthesis from syngas over Rh-based/SiO_2 catalysts: a combined experimental and theoretical modeling study. *J Catal*. 2010;271:325–342.
13. Zaman S, Smith KJ. A review of molybdenum catalysts for synthesis gas conversion to alcohols: catalysts, mechanisms and kinetics. *Catal Rev Sci Eng*. 2012;54:41–132.
14. Razzaghi A, Hindermann JP, Kiennemanna A. Synthesis of C1 to C5 alcohols by CO+H_2 reaction on some modified iron-catalysts. *Appl Catal*. 1984;13:193–210.
15. Nunan JG, Bogdan CE, Klier K, Smith KJ, Young CW, Herman RG. Methanol and C_2 oxygenate synthesis over cesium doped Cu-ZnO and Cu/ZnO/Al_2O_3 catalysts: a study of selectivity and ^{13}C incorporation patterns. *J Catal*. 1988;113:410–433.
16. Bian G, Fan L, Fu Y, Fujimoto K. Mixed alcohol synthesis from syngas on sulfided K-Mo-based catalysts: influence of support acidity. *Ind Eng Chem Res*. 1998;37:1736–1743.
17. Xiao K, Qi X, Bao Z, Wang X, Zhong L, Fang K, Lin M, Sun Y. CuFe, CuCo and CuNi nanoparticles as catalysts for higher alcohol synthesis from syngas: a comparative study. *Catal Sci Technol*. 2013;3:1591–1602.
18. Beretta A, Sun Q, Herman RG, Klier K. Production of methanol and isobutyl alcohol mixtures over double-bed cesium-promoted Cu/ZnO/Cr_2O_3 and ZnO/Cr_2O_3 catalysts. *Ind Eng Chem Res*. 1996;35:1534–1542.
19. Smith KJ, Anderson RB. The higher alcohol synthesis over promoted Cu/ZnO catalysts. *Can J Chem Eng*. 1983;61:40–45.
20. Mahdavi V, Peyrovi MH, Islami M, Mehr JY. Synthesis of higher alcohols from syngas over Cu-Co_2O_3/ZnO, Al_2O_3 catalyst. *Appl Catal A*. 2005;281:259–265.
21. Wang J, Chernavskii PA, Khodakov AY, Wang Y. Structure and catalytic performance of alumina-supported copper-cobalt catalysts for carbon monoxide hydrogenation. *J Catal*. 2012;286:51–61.
22. Chaumette P, Courty Ph, Kiennemann A, Kieffer R, Boujana S, Martin GA, Dalmon JA, Meriaudeau P, Mirodatos C. Evolution of alcohol synthesis catalysts under syngas. *Ind Eng Chem Res*. 1994;33:1460–1467.
23. Forzatti P, Tronconi E, Pasquon I. Higher alcohol synthesis. *Catal Rev Sci Eng*. 1991;33:109–168.
24. Iglesia E. Design, synthesis, and use of cobalt-based Fischer-Tropsch synthesis catalysts. *Appl Catal A*. 1997;161:59–78.

25. Weckhuysen BM. Promotion effects in Co-based Fischer-Tropsch catalysis. In: Morales F, editor. *Catalysis*. London: The Royal Society of Chemistry, 2006:1–40.
26. de Aquino AD, Cobo AJG. Synthesis of higher alcohols with cobalt and copper based model catalysts: effect of the alkaline metals. *Catal Today*. 2001;65:209–216.
27. Tien-Thao N, Zahedi-Niaki MH, Alamdari H, Kaliaguine S. Effect of alkali additives over nanocrystalline Co-Cu-based perovskites as catalysts for higher-alcohol synthesis. *J Catal*. 2007;245:348–357.
28. Tien-Thao N, Alamdari H, Zahedi-Niaki MH, Kaliaguine S. $LaCo_{1-x}Cu_xO_{3-\delta}$ perovskite catalysts for higher alcohol synthesis. *Appl Catal A*. 2006;311:204–212.
29. Rocha AL, Solórzano IG, Vander Sande JB. Heterogeneous and homogeneous nanoscale precipitation in dilute Cu-Co alloys. *Mater Sci Eng C*. 2007;27:1215–1221.
30. Smith ML, Kumar N, Spivey JJ. CO adsorption behavior of Cu/SiO_2, Co/SiO_2, and CuCo/SiO_2 catalysts studied by in situ DRIFTS. *J Phys Chem C*. 2012;116:7931–7939.
31. Carenco S, Tuxen A, Chintapalli M, Pach E, Escudero C, Ewers TD, Jiang P, Borondics F, Thornton G, Alivisatos AP, Bluhm H, Guo J, Salmeron M. Dealloying of cobalt from CuCo nanoparticles under syngas exposure. *J Phys Chem C*. 2013;117:6259–6266.
32. Wojciechowski BW. The kinetics of the Fischer-Tropsch synthesis. *Catal Rev Sci Eng*. 1988;30:629–702.
33. Mo X, Tsai YT, Gao J, Mao D, Goodwin JG Jr. Effect of component interaction on the activity of Co/CuZnO for CO hydrogenation. *J Catal*. 2012;285:208–215.
34. Surisetty VR, Dalai AK, Kozinski J. Intrinsic reaction kinetics of higher alcohol synthesis from synthesis gas over a sulfided alkali-promoted Co-Rh-Mo trimetallic catalyst supported on multiwalled carbon nanotubes (MWCNTs). *Energy Fuels*. 2010;24:4130–4137.
35. Frossling N. The evaporation of falling drops. *Gerlands Beitr Geophys*. 1938;52:170–216.
36. Weisz PB, Prater CD. Interpretation of measurements in experimental catalysis. *Adv Catal*. 1954;6:143–196.
37. Ertl G, Knözinger H, Schüth F, Weitkamp J. *Handbook of Heterogeneous Catalysis*. Weinheim, Germany: Wiley-VCH, 2008.
38. Smith ML, Campos A, Spivey JJ. Reduction processes in Cu/SiO_2, Co/SiO_2, and CuCo/SiO_2 catalysts. *Catal Today*. 2012;182:60–66.
39. Fischer N, van Steen E, Claeys M. Structure sensitivity of the Fischer-Tropsch activity and selectivity on alumina supported cobalt catalysts. *J Catal*. 2013;299:67–80.
40. Kasatkin I, Kurr P, Kniep B, Trunschke A, Schlögl R. Role of lattice strain and defects in copper particles on the activity of Cu/ZnO/Al_2O_3 catalysts for methanol synthesis. *Angew Chem*. 2007;119:7465–7468.
41. Mei D, Rousseau R, Kathmann SM, Glezakou VA, Engelhard MH, Jiang W, Wang C, Gerber MA, White JF, Stevens DJ. Ethanol synthesis from syngas over Rh-based/SiO_2 catalysts: a combined experimental and theoretical modeling study. *J Catal*. 2010;271:325–342.
42. Xiao K, Bao Z, Qi X, Wang X, Zhong L, Fang K, Lin M, Sun Y. Advances in bifunctional catalysis for higher alcohol synthesis from syngas. *Chin J Catal*. 2013;34:116–129.
43. Prieto G, Concepción P, Martínez A, Mendoza E. New insights into the role of the electronic properties of oxide promoters in Rh-catalyzed selective synthesis of oxygenates from synthesis gas. *J Catal*. 2011;280:274–288.
44. Li J, Zhan X, Zhang Y, Jacobs G, Das T, Davis BH. Fischer–Tropsch synthesis: effect of water on the deactivation of Pt promoted Co/Al_2O_3 catalysts. *Appl Catal A*. 2002;228:203–212.
45. Yuan W, Zhu K. *Analysis of Chemical Reaction Engineering*. Shanghai: East China University of Science and Technology Press, 1994.
46. Xiang Y, Chitry V, Liddicoat PV, Felfer P, Cairney J, Ringer S, Kruse N. Long-chain terminal alcohols through catalytic CO hydrogenation. *J Am Chem Soc*. 2013;135:7114–7117.
47. Fang YZ, Liu Y, Zhang LH. $LaFeO_3$-supported nano Co-Cu catalysts for higher alcohol synthesis from syngas. *Appl Catal A*. 2011; 397:183–191.
48. Saib AM, Borgna A, van de Loosdrecht J, van Berge PJ, Geus JW, Niemantsverdriet JW. Preparation and characterization of spherical Co/SiO_2 model catalysts with well-defined nano-sized cobalt crystallites and a comparison of their stability against oxidation with water. *J Catal*. 2006;239:326–339.
49. Concepción P, López C, Martínez A, Puntes VF. Characterization and catalytic properties of cobalt supported on delaminated ITQ-6 and ITQ-2 zeolites for the Fischer-Tropsch synthesis reaction. *J Catal*. 2004;228:321–332.
50. Chu W, Chernavskii PA, Gengembre L, Pankina GA, Fongarland P, Khodakov AY. Cobalt species in promoted cobalt alumina-supported Fischer–Tropsch catalysts. *J Catal*. 2007;252:215–230.
51. Martínez A, Prieto G, Rollán J. Nanofibrous γ-Al_2O_3 as support for Co-based Fischer-Tropsch catalysts: pondering the relevance of diffusional and dispersion effects on catalytic performance. *J Catal*. 2009;263:292–305.
52. Hansen JB, Højlund Nielsen PE. Methanol synthesis. In: Ertl G, Knözinger H, Schüth F, Weitkamp J, editors. *Handbook of Heterogeneous Catalysis*, 2nd ed. Weinheim: Wiley-VCH, 2008:2920–2949.
53. Behrens M, Studt F, Kasatkin I, Kühl S, Hävecker M, Abild-Pedersen F, Zander S, Girgsdies F, Kurr P, Kniep BL, Tovar M, Fischer RW, Nørskov JK, Schlögl R. The active site of methanol synthesis over Cu/ZnO/Al_2O_3 industrial catalysts. *Science*. 2012;336:893–897.
54. Jacobs G, Ribeiro MC, Ma W, Ji Y, Khalid S, Sumodjo PTA, Davis BH. Group II (Cu, Ag, Au) promotion of 15%Co/Al_2O_3 Fischer-Tropsch synthesis catalysts. *Appl Catal A*. 2009;361:137–151.
55. Nørskov JK, Abild-Pedersen F, Studt F, Bligaard T. Density functional theory in surface chemistry and catalysis. *Proc Natl Acad Sci USA*. 2011;108:937–943.
56. Mouaddib N, Perrichon V, Martin GA. Characterization of copper-cobalt catalysts for alcohol synthesis from syngas. *Appl Catal A*. 1994;118:63–72.
57. Li G, Wang Q, Li D, Lü X, He J. Structure evolution during the cooling and coalesced cooling processes of Cu-Co bimetallic clusters. *Phys Lett A*. 2008;372:6764–6769.
58. Ahmed J, Ganguly A, Saha S, Gupta G, Trinh P, Mugweru AM, Lofland SE, Ramannujachary KV, Ganguli AK. Enhanced electrocatalytic activity of copper-cobalt nanostructures. *J Phys Chem C*. 2011;115:14526–14533.
59. Edelstein AS, Harris VG, Rolinson DR, Kurihara L, Smith DJ, Perepezko J, da Silva Bassani MH. Inversion of surface composition and evolution of nanostructure in Cu/Co nanocrystals. *Appl Phys Lett*. 1999;74:3161–3164.
60. Wilson J, de Groot C. Atomic-scale restructuring in high-pressure catalysis. *J Phys Chem*. 1995;99:7860–7866.
61. Prieto G, Martínez A, Concepción P, Moreno-Tost R. Cobalt particle size effects in Fischer–Tropsch synthesis: structural and in situ spectroscopic characterisation on reverse micelle-synthesised Co/ITQ-2 model catalysts. *J Catal*. 2009;266:129–144.
62. Ciobîcă IM, van Santen RA, van Berge PJ, van de Loosdrecht J. Adsorbate induced reconstruction of cobalt surfaces. *Surf Sci*. 2008; 602:17–27.
63. Vollmer S, Witte G, Wöll C. Determination of site specific adsorption energies of CO on copper. *Catal Lett*. 2001;77:97–101.
64. Liao K, Fiorin V, Gunn DSD, Jenkins SJ, King DA. Single-crystal adsorption calorimetry and density functional theory of CO chemisorption on fcc Co{110}. *Phys Chem Chem Phys*. 2013;15:4059–4065.
65. Bailliard-Letournel RM, Cobo AJG, Mirodatos C, Primet M, Dalmon JA. About the nature of the Co-Cu interaction in Co-based catalysts for higher alcohols synthesis. *Catal Lett*. 1989;2: 149–156.
66. Chaumette P, Courty Ph, Kiennemann A, Ernst B. Higher alcohol and paraffin synthesis on cobalt based catalysts: comparison of mechanistic aspects. *Top Catal*. 1995;2:117–126.
67. Volkova GG, Yurieva TM, Plyasova LM, Naumova MI, Zaikovskii VI. Role of the Cu-Co alloy and cobalt carbide in higher alcohol synthesis. *J Mol Catal A*. 2000;158:389–393.
68. Biloen P, Sachtler WMH. Mechanism of hydrocarbon synthesis over Fischer-Tropsch catalysts. *Adv Catal*. 1981;30:165–216.
69. van Santen RA, Markvoort AJ, Ghouri MM, Hilbers PAJ, Hensen EJM. Monomer formation model versus chain growth model of the Fischer-Tropsch reaction. *J Phys Chem C*. 2013;117:4488–4504.
70. van Santen RA, Ciobica IM, van Steen E, Ghouri MM. Mechanistic issues in Fischer-Tropsch catalysis. *Adv Catal*. 2011;54:127–187.
71. Bezemer GL, Bitter JH, Kuipers HPCE, Oosterbeek H, Holewijn JE, Xu X, Kapteijn F, van Dillen AJ, de Jong KP. Cobalt particle size effects in the Fischer-Tropsch reaction studied with carbon nanofiber supported catalysts. *J Am Chem Soc*. 2006;128:3956–3964.
72. Den Breejen JP, Sietsma JRA, Friedrich H, Bitter JH, de Jong KP. Design of supported cobalt catalysts with maximum activity for the Fischer-Tropsch synthesis. *J Catal*. 2010;270:146–152.
73. Feng W, Wang Q, Jiang B, Ji P. Carbon nanotubes coated on silica gels as a support of Cu-Co catalyst for the synthesis of higher alcohols from syngas. *Ind Eng Chem Res*. 2011;50:11067–11072.

74. Prieto G, Martínez A, Murciano R, Arribas MA. Cobalt supported on morphologically tailored SBA-15 mesostructures: the impact of pore length on metal dispersion and catalytic activity in the Fischer-Tropsch synthesis. *Appl Catal A*. 2009;367:146–156.
75. Den Breejen JP, Frey AM, Yang J, Holmen A, van Schooneveld MM, de Groot FMF, Stephan O, Bitter JH, de Jong KP. A highly active and selective manganese oxide promoted cobalt-on-silica Fischer-Tropsch catalyst. *Top Catal*. 2011;54:768–777.
76. van Hardeveld R, van Montfoort A. The influence of crystallite size on the adsorption of molecular nitrogen on nickel, palladium and platinum: an infrared and electron-microscopic study. *Surf Sci*. 1966; 4:396–430.
77. Ciobîcă IM, van Santen RA. Carbon monoxide dissociation on planar and stepped Ru(0001) surfaces. *J Phys Chem B*. 2003;107:3808–3812.
78. Dahl S, Logadottir A, Egeberg RC, Larsen JH, Chorkendorff I, Törnqvist E, Nørskov JK. Role of steps in N_2 activation on Ru(0001). *Phys Rev Lett*. 1999;83:1814–1817.

Manuscript received Aug. 22, 2013, and revision received Dec. 24, 2013.